International Journal of Rotating Machinery
2000, Vol. 6, No. 3, pp. 167–180
Reprints available directly from the publisher
Photocopying permitted by license only

Laser Velocimeter Measurements in the Pump of an Automotive Torque Converter Part I – Effect of Speed Ratio

STEVEN B. AINLEY, RONALD D. FLACK*, KLAUS BRUN and TONY J. ROVELLO

Department of Mechanical, Aerospace, and Nuclear Engineering, University of Virginia, Charlottesville, VA 22903-2442, USA

(Received 30 June 1997; In final form 31 July 1998)

A torque converter was tested at four turbine/pump rotational speed ratios (0.200, 0.400, 0.600, and 0.800) all with a constant pump rotational speed in order to determine the effect of speed ratio on the torque converter pump flow field. Laser velocimetry was used to measure three components of velocity within the pump and a shaft encoder was employed to record the instantaneous pump angular position. Shaft encoder information was correlated with measured velocities to develop flow field blade-to-blade profiles and vector plots. Measurements were obtained in both the pump mid- and exit planes for all four speed ratios. Results showed large separation regions and jet/wake flows throughout the pump. The mid-plane flow was found to have strong counter-clockwise secondary components and the exit plane flow had strong clockwise secondary components. Mass flows were calculated from the velocity data and were found to decrease as the speed ratio was increased. Also, the vorticity and slip factors were calculated from the experimental data and are included. The mid-plane slip factors compare favorably to those for conventional centrifugal pumps but less slip was present in the exit plane than the mid-plane. Neither the slip factor nor the vorticity were seen to be strongly affected by the speed ratio. Finally, the torque core-to-shell and blade-to-blade torque distributions are presented for both planes.

Keywords: Torque converters, Pumps, Laser velocimetry

INTRODUCTION

The torque converter, commonly used in automobiles, is a hydrodynamic turbomachine which transmits torque smoothly between the engine and the transmission, provides torsional damping, and reduces the shock resulting from sudden changes in operating conditions. The typical torque converter consists of a pump, a turbine, and a stator, and employs oil as the working fluid. The pump is driven by the engine via the crankshaft and energizes the working fluid. The energized fluid

* Corresponding author. Tel.: (804) 924 6213. Fax: (804) 982 2037. E-mail: rdf@virginia.edu.

exits the pump axially and enters the turbine, which extracts energy from the fluid. The stator is the non-rotating component of the torque converter and is located between the turbine exit and pump inlet. The stator is designed to redirect the flow exiting the turbine into the pump with zero incidence angle at the "design" condition. The oil is continually recirculated through the pump, turbine, and the stator.

The torque converter is a very complex turbomachine for several reasons. First, the flow field changes dramatically over the range of operating conditions. Specifically, incidence angles to the leading edge of the blades for all of the components change from large positive to large negative values over the operating range. Second, the flow is highly three-dimensional as it is turned in the blade passages in two directions. Thus, as in any turbomachine, blade slip becomes a problem, especially at off-design operating conditions. Also, in addition to turning in the tangential and radial directions, the flow is turned by 180° in the transverse axial direction in both the pump and the turbine in a relatively short distance. Namely, the flow enters these two components in the axial direction, is rapidly turned toward the radial direction, and rapidly turned back into the reverse axial direction. Thus, the torque converter is a very complex mixed-flow variety of hydraulic turbomachine.

Previous Work

A detailed review of early torque converter work was given by Bahr *et al.* (1990), Gruver *et al.* (1996) and Brun *et al.* (1996) and Brun and Flack (1996). Thus, for the sake of brevity only some of the more recent publications on torque converters are reviewed herein.

Browarzik and Grahl (1992), and Browarzik (1994) examined the non-steady flow field at the pump and turbine inlet and outlet using hot-film anemometry. A frequency spectrum showing the relative magnitudes of velocities at the turbine exit was presented. Relative velocity magnitude as a function of pump and turbine angular position was also shown. Folchert *et al.* (1994) presented a mathematical description of the nonlinear behavior of hydrodynamic torque converters. Linear models in the frequency and time domain for each region were established by identification methods and frequency response curves for the driving system can then be calculated with high accuracy. An inverse Fourier transformation into the time domain allows the calculation of the dynamic behavior due to general transient excitations.

Hedman (1994) presented different ways of implementing the torque converter's non-linear relationships for torque and speeds into a computational model. He presented ways of combining the non-linear torque converter relationships with linear relationships for the rest of the transmission in order to calculate the speeds and torque of all shafts in the entire transmission system. Schultz *et al.* (1994) described a finite volume method for calculating three-dimensional incompressible viscous flow in a torque converter. Calculations were done in the guide vane, pump rotor, and turbine rotor of a torque converter and the method was shown to be an effective tool for the prediction of turbomachinery flows.

Marathe *et al.* (1996) and Marathe and Lakshminarayana (1995) used a five-hole probe to acquire pressure data at the turbine exit and stator exit of a torque converter. The flow fields were found to be highly three-dimensional and strong secondary flows were found. A separation region near the shell side of the stator passage was observed. The experimental data was in good agreement with the Navier–Stokes computational predictions at the stator exit for both "design" and "off-design" conditions.

Wantanabe *et al.* (1997) used flow visualization and laser velocimetry to study the flow in stator passages for different thicknesses of vanes. They found that the thickness affected the flow fields and other parameters including the flow rate. They also found that the flow was non-uniform and separated regions were present regardless of the test conditions.

Bahr *et al.* (1990) measured velocity fields in three dimensions throughout the stator of the torque converter. For the study, a one directional laser

velocimeter was used to measure in a machined Plexiglas torque converter. The inlet, one-quarter, mid-, three-quarter, and exit planes were studied using a resolution of 5 by 5 measurement locations for speed ratios of 0.065 and 0.800. At the 0.800 speed ratio a separation region was observed in the mid-plane at the pressure and core sides. For the same speed ratio another separation region was observed in the exit plane at suction and shell sides. The flow rates and torque distributions were found to be strongly dependent on radial position.

Gruver *et al.* (1996) and Brun *et al.* (1996) used the same experimental facility as Bahr *et al.* (1990) to measure steady and unsteady velocities in the pump of the torque converter. Three-dimensional velocity fields were measured in the inlet, mid-, and exit planes of the pump at the speed ratios of 0.065 and 0.800 and pump rotational speed of 800 and 1100 rpm. The flow field in the pump inlet was found to be strongly dependent on the relative position between the pump and the stator. The pump exit velocity field was found to be influenced by the relative position between the pump and the turbine. Secondary flow was found in all three planes with the most significant occurring in the mid- and exit planes at the 0.800 speed ratio. Large separation regions were shown in the mid- and exit planes at the core and suction sides at both speed ratios. The pump inlet and exit flow field were seen to be highly unsteady.

Brun *et al.* (1996) used the same experimental facility as Bahr *et al.* (1990) to measure velocity fields in the turbine of the torque converter. The speed ratios of 0.065 and 0.800 were studied for the inlet, one-quarter, mid-, and exit planes of the turbine. Average flow velocity profiles were obtained for all the measurement planes and transient velocity fields were determined for all the planes except for the exit plane. The relative pump-turbine position exhibited a strong influence on the turbine inlet flow for both speed ratios. Significant separation regions were found in the one-quarter and mid-planes at the 0.065 speed ratio.

By and Lakshminarayana (1995), By *et al.* (1995), and By (1993) studied a torque converter with the same geometry as Bahr *et al.* (1990). Steady pressure measurements were taken in both the stator and pump. These measurements were compared with both a potential flow analysis and a numerical viscous flow prediction and agreed favorably with the results. The viscous flow prediction was used to show that the pump rotation with the radially curved channel precipitated a strong secondary flow.

Motivations and Objectives

Torque converters are used extensively in the automotive industry. However, their internal flow characteristics are not well understood and have received little attention, particularly over a wide range of operating conditions. Theoretical analysis of the torque converter has not developed to a level permitting design solely from computational results. Detailed velocity field experimental data, including velocity distribution, pressures, and turbulence intensities, are required for benchmarking and as boundary/initial conditions for computational flow solvers.

The motivation for research in the torque converter pump is three-fold: (i) The current design methods need to be improved in order to advance torque converter technology significantly; namely, velocity data is needed as a benchmark for verification of flow models. (ii) Since the torque converter operates very inefficiently at off-design conditions, optimization of the internal flow paths will yield an improved torque converter and better automobile fuel efficiency. A greater understanding of the fundamental flow behavior is required to design improved blade passages. (iii) Torque converter pumps are extremely complex mixed-flow turbomachines because radial, axial, and tangential flow components are present. A basic understanding of its mixed-flow behavior at different operating conditions can be directly related to other mixed flow turbomachines.

A laser velocimeter was used in this study to non-intrusively measure velocity components in the pump of a Plexiglas model automotive torque

converter. Velocities were measured in the mid- and exit planes at four speed ratios (turbine rotational speed/pump rotational speed) with a constant pump rotational speed and results are related to this speed ratio parameter. From the velocity data, flow non-uniformities and, in particular, separated regions were determined. Mass flow rates and mass flux distributions in each plane were calculated from the velocity data. Also, slip factors and non-dimensional vorticities were calculated at the mid- and exit planes. Finally, torque flux distribution was calculated for both planes. The use of the obtained experimental results should lead to improved computational modeling of the flow field in the torque converter.

EXPERIMENTAL FACILITY

Torque Converter Rig

The entire experimental apparatus is shown schematically in Fig. 1. The torque converter pump was driven by a 18.6 kW motor and the rotational energy from the torque converter turbine was absorbed by a 130.5 kW eddy current dynamometer. A hydraulic system cooled, lubricated, and pressurized the torque converter rig. The pressures and temperatures throughout the test fixture and support system were monitored and controlled. The pump and turbine rotational speeds were controlled to within 1 rpm. The input and output torque were measured by load cells on the shafts and displayed on the console.

The torque converter tested was a standard single stage automotive model with a diameter of 230 mm and was manufactured entirely of Plexiglas for optical accessibility. The torque converter was located in a rectangular containment box also made of Plexiglas as shown in Fig. 2. Both the torque converter and containment box were filled with Shellfiex 212 industrial oil, which has an index of refraction of 1.489 at 25°C. This oil was chosen because it matched the index of refraction of the Plexiglas (nominally 1.490), which reduced undesired laser beam refraction, reflection, and scattering. The density of the oil at 25°C is 899.1 kg/m^3 and the viscosity is 29 cSt at 25°C and 19 cSt at 40°C.

The torque converter pump consisted of 27 identical blade passages, the turbine of 29 identical blade passages, and the stator of 19 passages. The pump blades were constructed by milling a solid piece of Plexiglas and thus creating a one piece "nest" with the blades an integral part of the core. The blade nest was then permanently attached to a separately constructed pump shell with a solvent. The same process was used to construct the turbine. The pump and turbine blades were 1.1 mm thick and the shells were 2.67 mm thick. The stator blades and shell were also milled from a single piece of Plexiglas and then glued to the core. In Fig. 3 the

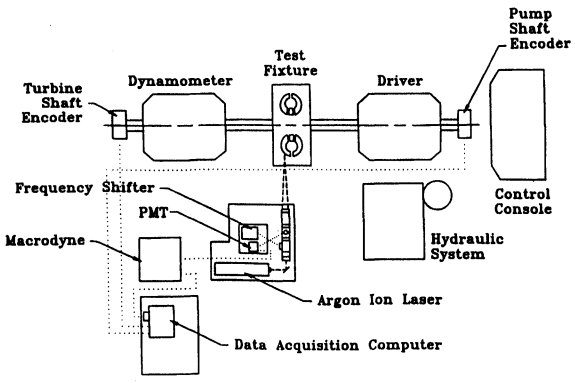

FIGURE 1 Experimental facility.

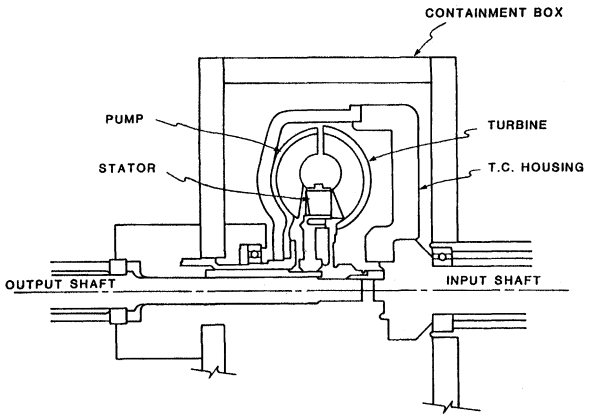

FIGURE 2 Plexiglas torque converter and containment box.

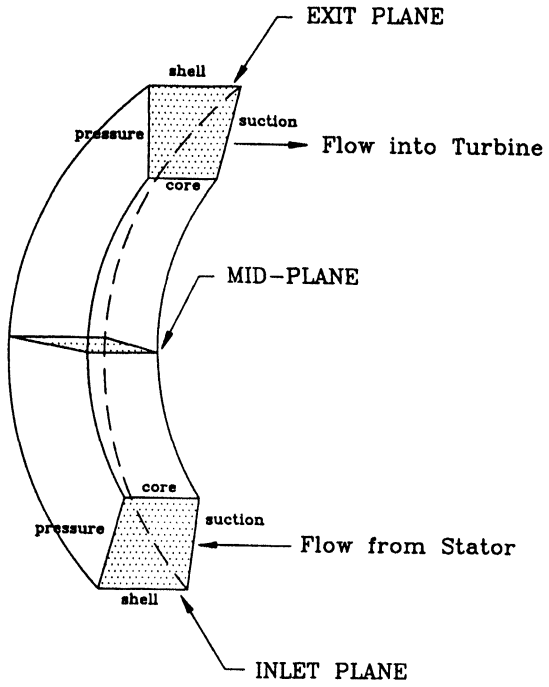

FIGURE 3 Pump passage geometry.

pump geometry and the two measurement planes are shown. The blade passage geometries and operating conditions were previously fully documented by By and Lakshminarayana (1995), Gruver *et al.* (1996), and By (1993). Thus, the entire test-facility can be reconstructed from information in the public domain. Also, the performance curves for the tested torque converter geometry are presented in Fig. 4.

LV System

A one-directional, frequency shifted, back scatter laser velocimeter system was used for this study. A 2-watt Argon-Ion laser, operated at 50 mW and at a wavelength of 514.5 nm, was employed. The laser and the accompanying laser velocimeter optics were mounted on a mill table as shown in Fig. 5 to provide a stable vibration free base. The position of the table and, thus, the measurement location (probe volume) was controlled by 3-axis stepper motors, linear encoders, and a digital read-out.

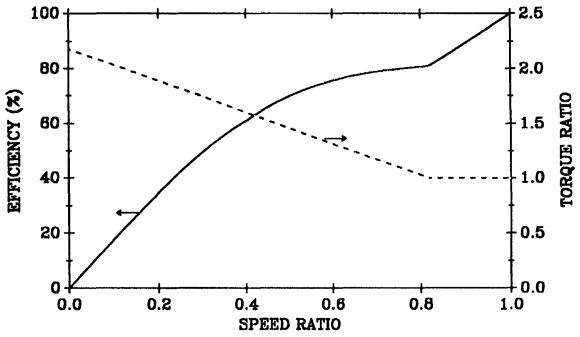

FIGURE 4 Torque converter power efficiency and torque ratio.

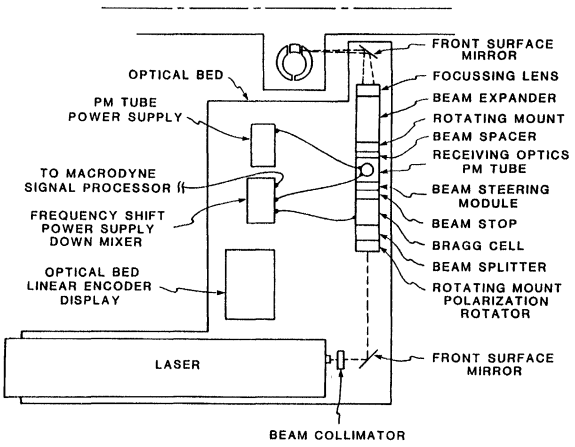

FIGURE 5 Laser velocimeter and optics installed on mill table.

The single laser beam from the emission source was split into two equal intensity beams by a beam splitter module. One beam was frequency upshifted using a Bragg Cell in order to eliminate velocity directional ambiguity. Beam spacers, expanders, and a focusing lens (focal length of 250 or 350 mm, depending on the measurement requirements) were employed to first reduce the probe volume size and then focus the laser beams to cross in the test section. To provide for light scattering, the oil was seeded with metallic coated glass particles which have an average diameter of 12 μm and have a density approximately that of the oil. The scattered light from the particles was focused into a 0.02 mm diameter pin-hole and then converted to a voltage signal by a photomultiplier tube (PMT). The PMT

output signal (Doppler signal) was amplified, sent to a burst counter processor, and converted to digital velocity output. The burst counter processor employed bandpass filtering, an adjustable minimum threshold, and a 5/8 peak counter comparator to validate burst signals. The digital velocity information was read into a data acquisition computer via a high speed digital I/O card. Simultaneously with each velocity signal, the instantaneous angular positions of the pump and turbine were read in using two 10-bit shaft encoders (1024 circumferential positions) attached to the pump and turbine shafts.

The measurement uncertainty of the velocity was due to the uncertainty of the clock counter in the digital processor, uncertainty in the beam crossing angle, and a the uncertainty of using a finite number of samples to approximate a true distribution; this uncertainty was typically ±0.05 m/s with 95% confidence. Uncertainties in the angular positions of the two rotating components were ±0.35°. Due to the small difference of index of refraction of the oil and plastic, a translational uncertainty of the probe volume position was also present and was approximately 0.05 mm. This probe volume position uncertainty was statistically added with the uncertainty in the angular position, which resulted in a typical uncertainty in the velocity of 0.07 m/s, when velocity gradients were present. As a consequence, the final total velocity uncertainty was 0.11 m/s.

Procedure

Measurement plane locations were determined by first using reference points in the pump and the known pump dimensions. The probe volume was then moved to the desired measurement locations in the pump with a total accuracy of the absolute position of 0.05 mm in any direction. In the pump mid- and exit planes, the velocity measurements were taken at 9 evenly spaced core-to-shell positions. Since the pump rotated, the velocity data for each core-to-shell position was resolved into 37 blade-to-blade positions. Therefore, for each pump plane a measurement grid of 9 core-to-shell by 37 blade-to-blade relative positions was obtained. Approximately 150 valid velocity samples were collected for each measurement grid position in the rotating frame, which is sufficient for a high confidence in the average velocities.

The pump was studied in detail for four speed ratios (0.200, 0.400, 0.600, and 0.800) with a constant pump rotational speed of 550 rpm in order to determine the effect of speed ratio on the torque converter flow field. Table I presents the different operating conditions. For reference, Reynolds numbers were also calculated for the pump exit plane for the various operating conditions and are included. The Reynolds number ($\mathrm{Re} = VD_h/\nu$) was calculated in two ways: (i) based on the through-flow velocity and (ii) based on the pump tip speed. In both methods of calculation, the hydraulic diameter, D_h, equals $4A/P$, where A is the area of the measurement plane and P is the wetted perimeter. The hydraulic diameter was 0.01901 m in the pump exit plane. For the Reynolds number calculation based on the through-flow, V is simply the average through-flow velocity in that plane, and for the calculation based on the tip speed, V is the velocity of the tip of the pump blade ($V = r\omega$).

Data Reduction

Average velocities were calculated and organized into blade-to-blade and core-to-shell profiles for the 27 blade passages of the pump using the pump

TABLE I Test conditions

Speed ratio	Pump speed (rpm)	Turbine speed (rpm)	Stator speed (rpm)	Temperature (°C)	Re (avg. thru flow)	Re (tip speed)
0.200	550	110	0	19	646	3901
0.400	550	220	0	19	548	3901
0.600	550	330	0	21	502	4107
0.800	550	440	0	25	433	4551

shaft encoder information. The velocity profiles of all blade passages were shown in studies not presented herein to be identical within the measurement uncertainties and, hence, could be superimposed and averaged. Blade-to-blade, core-to-shell velocity profiles, and vector plots were plotted using commercially available software.

RESULTS AND DISCUSSION

As previously described, experimental velocities were obtained for two pump planes at four turbine/pump rotational speed ratios. All velocities presented herein are given with respect to the rotating pump frame. Mass flows were calculated from the experimental through-flow velocity data, where through-flow velocity is defined as the velocity component normal to a given measurement plane. Secondary flows are also identified and quantified. Torque values are derived from the angular momentum fluxes and slip factors are determined from the relative tangential velocities. All of the above are presented and the effect of speed ratio on these parameters is discussed in detail.

Pump Mid-plane Velocity Fields

Velocity results for the 0.600 speed ratio mid-plane flow are presented in Figs. 6 and 7. Figure 6 shows a three-dimensional velocity vector plot of the flow field. Highest velocities (jet flow) can be seen to be along the shell side of the mid-plane and at the shell-pressure corner. The lowest velocities (wake flow) are located directly along the suction and core sides. The peak through-flow velocities at the shell-pressure side are approximately 2.7 times the average through-flow velocity. A significant flow separation region or wake is located near the suction side of the blade passage and extends towards the center of the plane. This jet/wake type flow is the result of a combination of Coriolis, centrifugal, and viscous forces, and was previously identified and described in detail for conventional centrifugal impellers by Eckardt (1975).

Figure 7 shows the secondary flow pattern of the mid-plane at the speed ratio of 0.600. Secondary flow is defined herein as the relative velocities (with respect to the pump frame) normal to the through-flow component. The secondary flows in the mid-plane are seen to have a strong counter-clockwise rotational circulation; average secondary velocities are 1.0 m/s. The region of highest secondary velocities is located at 40% pressure-to-suction and these velocities are approximately 1.2 m/s. Lowest secondary velocities are located in the core-suction corner region. The mid-plane velocity results for the other speed ratios have qualitatively similar jet/wake and circulatory secondary flow trends, but the

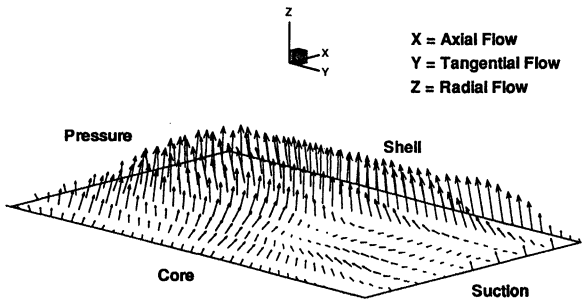

FIGURE 6 Pump mid-plane average total velocity vector plot for speed ratio 0.600.

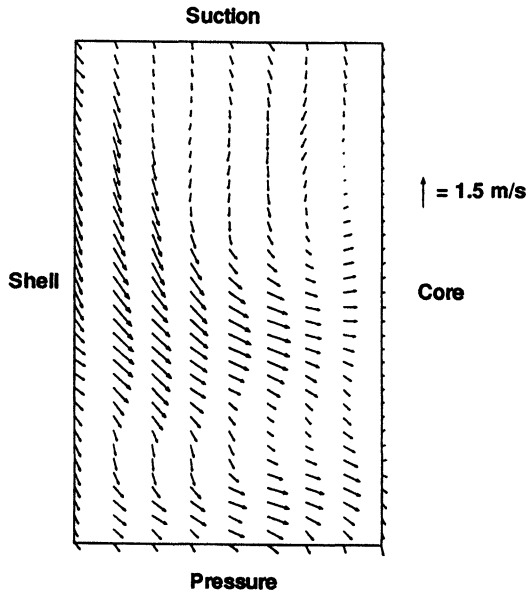

FIGURE 7 Pump mid-plane average secondary velocity vector plot for speed ratio 0.600.

magnitudes of the velocities magnitudes vary. Such plots are not presented for the sake of brevity but were documented by Ainley (1994).

For reference similar plots are presented in Figs. 8 and 9 for a speed ratio of 0.800. As can be seen, the general characteristics are the same as for the speed ratio of 0.600.

Pump Exit Plane Velocity Fields

Figure 10 shows the average exit plane vector plot at the 0.600 speed ratio. For this case, highest velocities are again located in the shell-pressure corner region and the lowest velocities are located near the suction side of the plane. The peak through-flow velocities are approximately 2.5 times the average through-flow velocity and are located near the shell-pressure corner. Velocities in the center of the plane are 1.2 times the average through-flow velocity. Along the core between 10–40% of the pressure-to-suction region, a triangular region of reversed flow is present. Thus, a jet/wake flow is still present in the exit plane.

Figure 11 shows the secondary flow pattern for the exit plane at the 0.600 speed ratio. The secondary flows in the exit plane have a strong clockwise rotational circulation, which is opposite that of the

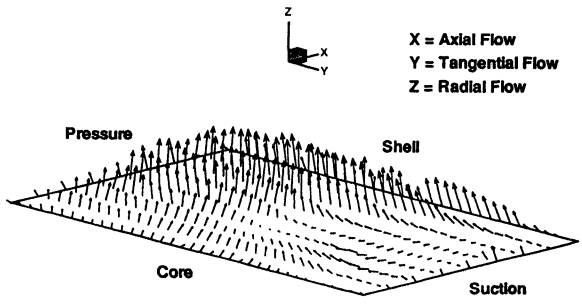

FIGURE 8 Pump mid-plane average total velocity vector plot for speed ratio 0.800.

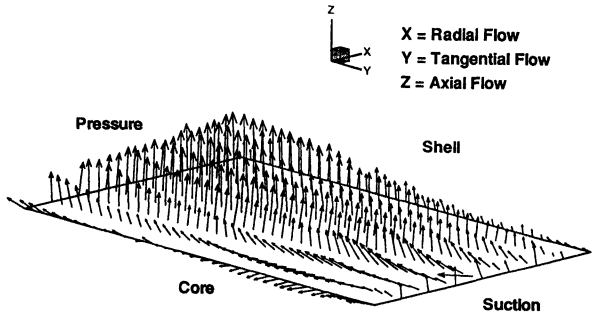

FIGURE 10 Pump exit plane average total velocity vector plot for speed ratio 0.600.

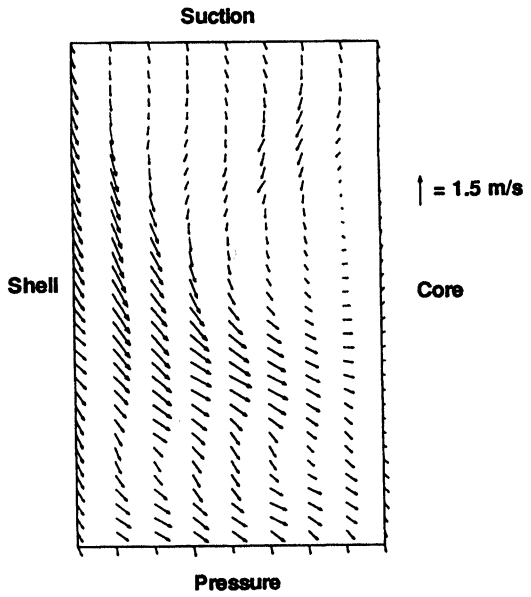

FIGURE 9 Pump mid-plane average secondary velocity vector plot for speed ratio 0.800.

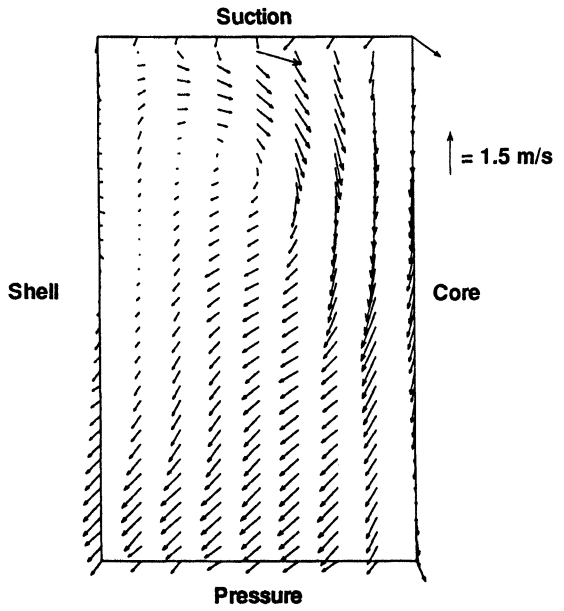

FIGURE 11 Pump exit plane average secondary velocity vector plot for speed ratio 0.600.

mid-plane. Hence, the circulatory secondary flows completely reversed their rotational direction between the mid- and exit-planes. Peak secondary flows are approximately 1.2 m/s and average secondary velocities in the exit plane are 0.9 m/s. A combined effect of both the Coriolis and centrifugal forces are believed to be responsible for the strong secondary flow in both the mid- and exit planes. The exit plane velocity results for the other speed ratios again have similar jet/wake and secondary flow trends but the magnitudes are different. Again, such plots are not presented for the sake of brevity but were documented previously by Ainley (1994).

For reference similar plots are presented in Figs. 12 and 13 for a speed ratio of 0.800. Once again, the general characteristics are the same as for the speed ratio of 0.600.

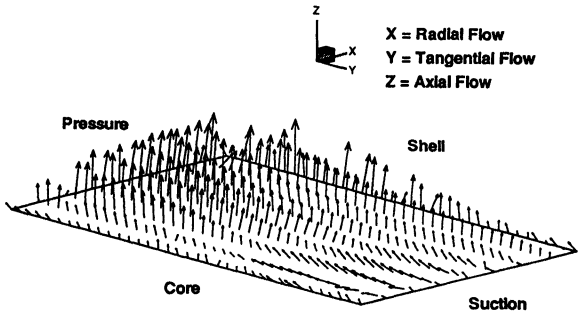

FIGURE 12 Pump exit plane average total velocity vector plot for speed ratio 0.800.

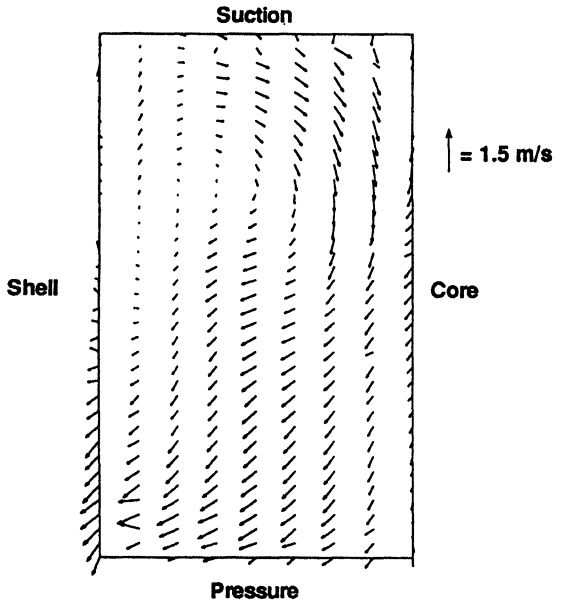

FIGURE 13 Pump exit plane average secondary velocity vector plot for speed ratio 0.800.

Mass Flux

The mass flows were calculated for the mid- and exit planes from the experimental data by integrating the through-flow velocity multiplied by the area and density across the entire measurement plane. The small differences between the mass flows from the mid-plane to the exit plane are well within the calculated mass flow uncertainties. The measured mass flow rate for the two planes and four speed ratios are shown in Fig. 14. The mass flow rate decreases by approximately 40% as the speed ratio is increased from 0.200 to 0.800.

Figure 15 shows the mass flux distribution from pressure-to-suction (blade-to-blade) for both planes at speed ratios of 0.200, 0.600, and 0.800. For this figure the mass flux was averaged from core to shell. For both planes, the highest mass flux is located at 10–15% of the pressure-to-suction surface. Near the suction side of the blade passage the mass flow is minimal and actually negative for high speed ratios in the mid-plane, indicating reverse flow. The core-to-shell mass flux distribution for both the mid- and exit planes at speed ratios of 0.200, 0.600, and 0.800 is shown in Fig. 16. Conversely, for this figure the mass flux was averaged from pressure to suction surface. For the highest speed ratios, near the core side of the blade passage the mass flux is approximately zero in the mid-plane and negative in the exit plane; the mass flux increases steadily towards the shell side of the passage in both planes. For the lowest speed ratio, the distribution is more symmetric, especially in the exit plane. For all cases and planes the magnitudes of the mass flux, decrease as the speed ratio increases.

Torque Flux Distribution

The total shaft torque can be calculated from the angular momentum principle and is given by the

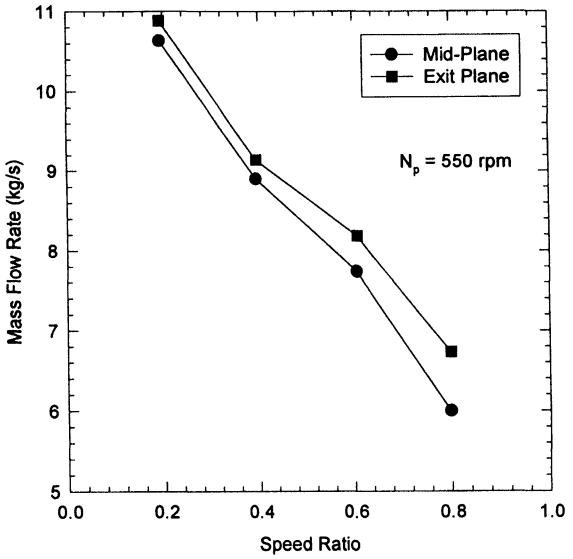

FIGURE 14 Pump mass flow rate as a function of speed ratio.

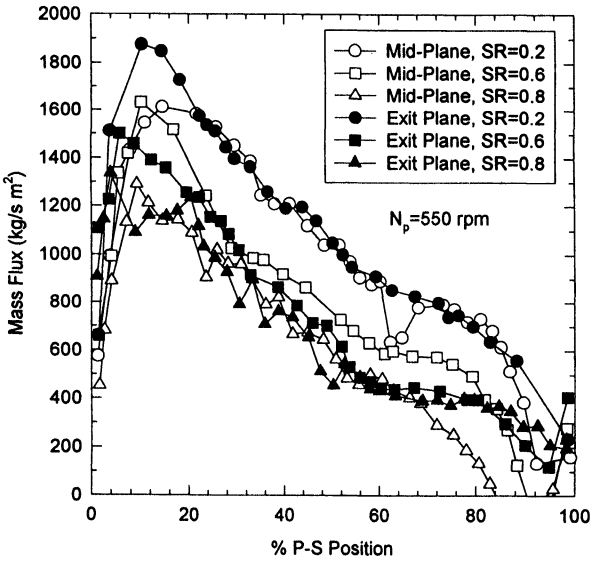

FIGURE 15 Pressure-to-suction surface mass flux distribution for speed ratios 0.200, 0.600, and 0.800.

equation:

$$T_{\text{shaft}} = \int_{cs} \vec{r} \times \vec{V} \rho \vec{V} \cdot d\vec{A}.$$

The torque flux distribution (N/m) or distribution of torque throughout the plane was determined by

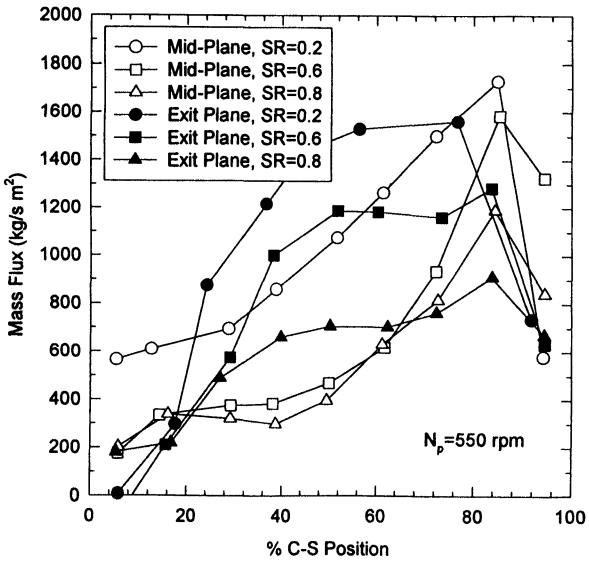

FIGURE 16 Core-to-shell surface mass flux distribution for speed ratios 0.200, 0.600, and 0.800.

calculating the torque contribution of each differential area as follows:

$$\text{Torque Flux} = \vec{r}_i \vec{V}_{\theta_i} \rho \vec{V}_{n_i},$$

where V_θ is the absolute tangential velocity, r_i is the radius from the shaft center, and V_n is the through-flow velocity. The pressure-to-suction (blade-to-blade) torque flux distribution for speed ratios of 0.200, 0.600, and 0.800 is shown in Fig. 17 for both the mid- and exit planes and the core-to-shell torque flux distribution is shown in Fig. 18. For these two figures the torque flux was averaged from core to shell and pressure to suction surface, respectively. The highest torque is located at approximately 10% pressure-to-suction and 80% core-to-shell in both the mid- and exit planes, regardless of speed ratio. Along the suction side and the core side of the blade passage, the torque flux is minimal. In the exit plane near the core surface and in the mid-plane near the suction surface the torque flux is negative for high speed ratios. Low torque flux regions indicate areas where minimal beneficial pump work is being done on the fluid. The magnitudes of the torque flux increase as the speed ratio decreases, as expected when considering the mass flux distribution.

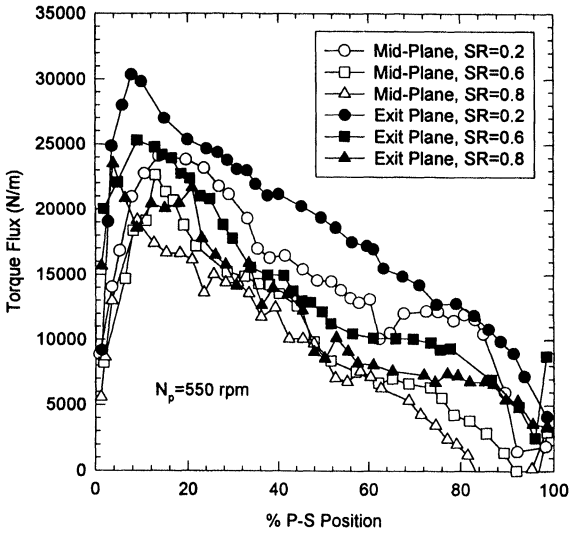

FIGURE 17 Pressure-to-suction surface torque flux distribution for speed ratios 0.200, 0.600, and 0.800.

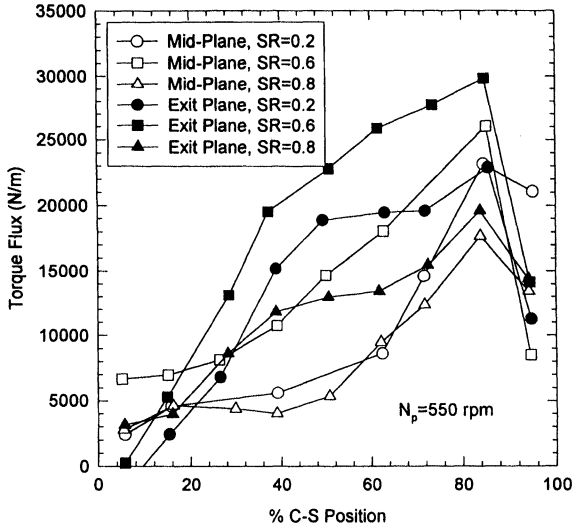

FIGURE 18 Core-to-shell surface torque flux distribution for speed ratios 0.200, 0.600, and 0.800.

Vorticity

The average flow vorticity, ξ, was calculated in the pump using the following equation:

$$\vec{\nabla}\xi = -\frac{1}{A}\iint (\vec{\nabla} \times \vec{v}) \cdot \mathrm{d}A$$
$$= -\frac{1}{A}\iint \left(\frac{\partial v}{\partial x} - \frac{\partial u}{\partial y}\right)\mathrm{d}A,$$

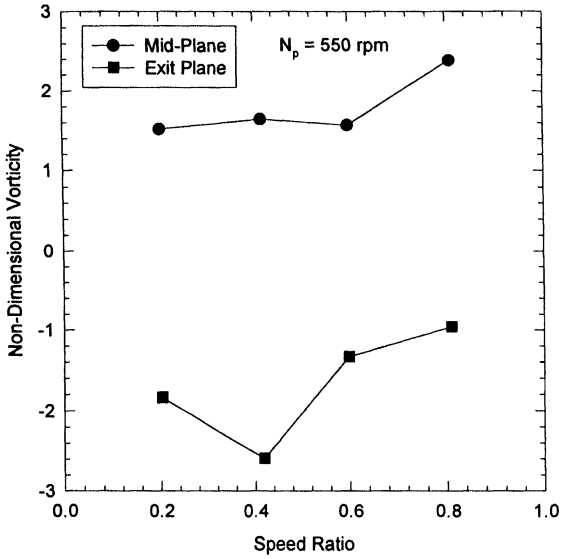

FIGURE 19 Pump non-dimensional vorticity as a function of speed ratio.

where u is the core-to-shell velocity and v is the pressure-to-suction velocity. The values of x and y are the absolute coordinates of the core-to-shell and pressure-to-suction locations, respectively. The vorticity equation in discretized form is

$$\xi = -\frac{1}{A}\sum_{i}^{n}\sum_{j}^{m}\left[\left(\frac{v_{j+1} - v_j}{x_{i+1} - x_i} - \frac{u_{j+1} - u_j}{y_{i+1} - y_i}\right) \times (x_{i+1} - x_i) \cdot (y_{i+1} - y_i)\right].$$

The vorticity, calculated from the above equation and the experimental data, was non-dimensionalized by dividing by the average through-flow velocity and multiplying by a reference length. The reference length for this calculation is the core-to-shell length of the pump blade (15.5 mm). The non-dimensional vorticity values are shown in Fig. 19 for both planes at the four speed ratios.

A positive vorticity value represents a secondary flow rotation in the counter-clockwise direction when looking directly into the plane from a downstream position. The highest mid-plane vorticity occurs at a speed ratio of 0.800 and the largest vorticity in the exit plane occurs at a speed ratio of

0.400. In the mid-plane the non-dimensional vorticities are seen to be relatively constant. In the exit plane the vorticity is lowest at a speed ratio of 0.800.

Slip Factor

The slip factor, μ is defined as the ratio of the actual fluid absolute tangential velocity to the ideal fluid tangential velocity. A slip factor equal to 1 indicates the tangential fluid flow perfectly matches the ideal flow. Since the pump blades in both the mid- and exit planes have a blade angle of approximately zero degrees, the ideal flow in both planes has a relative tangential velocity component equal to zero. The slip factor was calculated using the equation below,

$$\mu = \sum_i \frac{v_i + \omega r_i}{\omega r_i} \cdot \frac{w_i}{w_{\text{avg}}},$$

where v_i is the relative tangential fluid velocity, ω is the angular velocity in rad/sec, r_i is the radius of the measurement point, w_i is the through-flow velocity, and w_{avg} is the average through-flow velocity. The calculated values of slip are weighted by the through-flow velocity, as seen in the above equation. The pump slip factors are shown in Fig. 20 along with the values predicted for a 27-blade conventional centrifugal pump by Stodola (1945), Busemann (1928), and Wiesner (1967). The slip factors varied only slightly between the speed ratios, but the values in the exit plane are significantly higher than in the mid plane. The mid plane values range from 0.866 to 0.887 and the exit plane values range from 0.947 to 0.975.

The calculated values of the slip factor from measurements at the torque converter pump mid-plane are similar to the predicted values based on centrifugal pump data. This small difference can be attributed to the fact that, as previously indicated, the torque converter pump operates similar to a centrifugal pump especially in the inlet to mid plane section (the through-flow is in the radial direction). The values of the slip factor for the exit plane do not, however, agree as well with the predicted values. The measured slip factor values are significantly higher than the predicted values. The additional chord length from the mid-plane to the exit plane (nominal chord length between the inlet and exit plane is 2.2 times greater than from the inlet to the mid-plane) provides additional guidance to the flow and produces a higher slip factor (less slip) than for a normal centrifugal pump.

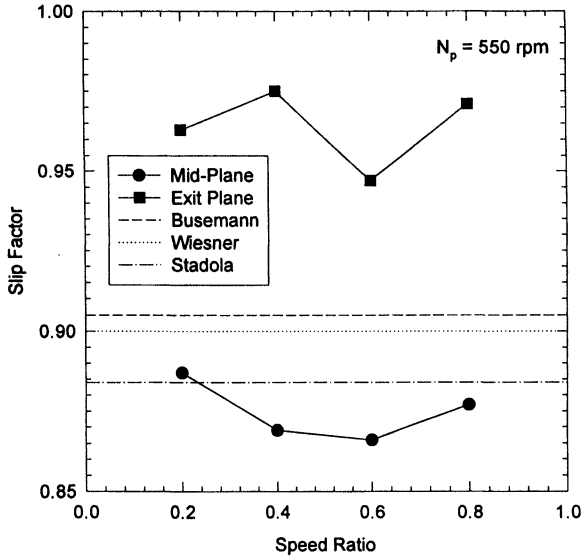

FIGURE 20 Pump slip factor as a function of speed ratio.

SUMMARY AND CONCLUSIONS

A laser velocimeter was used to measure the flow field in the mid- and exit planes of an automotive torque converter pump. Four speed ratios (0.200, 0.400, 0.600, and 0.800) were studied at a constant pump speed for both planes in order to determine the effect of speed ratio on the pump flow field. Important conclusions drawn from this investigation are:

1. In both measurement planes at all four speed ratios, the highest velocities (jet flow) are generally located at the pressure and shell sides of the blade passage. In the mid-plane, a separation (wake flow) region is located in the core-suction corner region and in the exit plane, a separation

region is located along the core side of the passage.

2. Mass flows were calculated for both planes at the four speed ratios. The calculated mass flows were consistent from the mid-plane to the exit plane. The measured mass flow was found to decrease from 10.8 kg/s to 6.8 kg/s in the pump exit plane and from 10.6 kg/s to 6.1 kg/s in the pump mid-plane as the speed ratio was increased from 0.200 to 0.800 (with a constant pump rotational speed). Core-to-shell and blade-to-blade mass flux distributions are also presented. In both the mid- and exit planes (all four speed ratios), the mass flux is highest near the pressure and shell sides of the blade passage.
3. The torque flux distribution was calculated for the mid- and exit planes in the pump. Torque flux distribution is similar to the mass flux distribution with the highest torque flux located at 10% pressure-to-suction and at 80% core-to-shell. The speed ratio does not have a significant influence on the torque flux distribution trends; however, the torque delivered to the pump increases as the speed ratio is decreased.
4. Strong secondary flow patterns are present in both the mid- and exit planes as is evident from the calculated vorticity values. The secondary flow is counter-clockwise in the mid-plane and clockwise in the exit plane. The circulation is a result of the combination of Coriolis, centrifugal and viscous forces. The strength of the secondary flow, as seen by the calculated vorticity, varies with the speed ratio and therefore, is mildly dependent upon the speed ratio. The strongest secondary flow (calculated non-dimensional vorticity is 2.42) in the mid-plane is at a speed ratio of 0.800 and the strongest secondary flow (calculated non-dimensional vorticity is -2.58) in exit plane is at a speed ratio of 0.400.
5. The slip factor in the torque converter pump was calculated and compared to predicted values for conventional centrifugal pumps. The calculated values at the mid-plane compared favorably with the predicted values. However, the pump exit plane slip factors were higher than predicted values. The added passage length adds to the fluid control, and thus reduces the amount of slip present at the exit plane. In both the mid- and exit planes, the slip factor was seen to be independent of the speed ratio.

Acknowledgments

This research was sponsored by General Motors Corporation Powertrain Division. The authors wish to express their gratitude to D. Maddock for his technical and hardware support. The research was also supported in part by the Rotating Machinery and Controls Laboratory at the University of Virginia.

References

Ainley, S.B. (1994) Laser velocimetry measurements in the stator and pump of an automotive torque converter, MS Thesis, University of Virginia.

Bahr, H.M., Flack, R.D., By, R.R. and Zhang, J.J. (1990) Laser velocimetry measurement in the stator of a torque converter, *SAE Paper No.* 901769, *SAE 1990 Transactions, Journal of Passenger Cars*, Vol. 99, Section 6, pp. 1625–1634.

Beaudoin, R.J., Miner, S.M. and Flack, R.D. (1989) Laser velocimeter measurements in a centrifugal pump with a synchronously orbiting impeller, *ASME Transactions, Journal of Turbomachinery*, Vol. 114, pp. 340–349.

Browarzik, V. and Grahl, K.G. (1992) Non-steady flow measurements inside a hydrodynamic torque converter by hot-film anemometry, *ASME International Gas Turbine and Aeroengine Congress and Exposition, ASME Paper No.* 92-GT-161.

Browarzik, V. (1994) Experimental investigation of rotor/rotor interaction in a hydrodynamic torque converter using hot film anemometry, *ASME International Gas Turbine and Aeroengine Congress and Exposition, ASME Paper No.* 94-GT-246.

Brun, K. (1993) Laser velocimeter measurements in a turbine of an automotive torque converter, MS Thesis, University of Virginia.

Brun, K. and Flack, R.D. (1994) A method to measure periodic velocity fields in multi-element turbomachines with discrete sampling, *Measurement Science and Technology*, Vol. 5, pp. 418–425.

Brun, K. and Flack, R.D. (1996) The flow field inside an automotive torque converter: Laser velocimeter measurements, *SAE Paper No.* 960721.

Brun, K., Flack, R.D. and Gruver, J.K. (1996) Laser velocimeter measurements in the pump of an automotive torque converter: Part II – Unsteady measurements, *ASME Transactions, Journal of Turbomachinery*, Vol. 118, pp. 570–577.

Busemann, A. (1928) Das förderhöhenverhältnis radialer kreiselpumpen mit logarithmisch-spiraligen schaufeln, *Zeitschrift für Angewandte Mathematik und Mechanik*, Vol. 8, pp. 372–384.

By, R.R. (1993) An investigation of three-dimensional flow fields in the automotive torque converter, doctoral dissertation, Pennsylvania State University.

By, R.R. and Lakshminarayana, B. (1995) Measurement and analysis of static pressure field in a torque converter pump, *ASME Transactions, Journal of Fluids Engineering*, Vol. 117, pp. 109–115.

By, R.R., Kunz, R.F. and Lakshminarayana, B. (1995) Navier stokes analysis of the pump of an automotive torque converter, *ASME Transactions, Journal of Fluids Engineering*, Vol. 117, pp. 116–122.

Eckardt, D. (1975) Instantaneous measurements in the jet-wake discharge flow of a centrifugal compressor impeller, *ASME Transactions, Journal of Engineering for Power*, Vol. 97, pp. 337–346.

Flack, R.D., Miner, S.M. and Beaudoin, R.J. (1989) Turbulence measurements in a centrifugal pump with a synchronously orbiting impeller, *ASME Transactions, Journal of Turbomachinery*, Vol. 111, pp. 350–359.

Fister, W. and Adrian, F.W. (1983) Experimental research of flow in hydrodynamic torque converters, *Proc. 7th Conf. on Fluid Machinery*, Budapest, Hungary, Vol. 1, pp. 210–224.

Folchert, U., Menne, A., and Waller, H. (1994) Experimental identification of the dynamic characteristic of hydrodynamic torque converters and Couplings, *ASME International Gas Turbine and Aeroengine Congress and Exposition, ASME Paper No.* 94-GT-360.

Gruver, J.K., Flack, R.D. and Brun, K. (1996) Laser velocimeter measurements in the Pump of a torque converter: Part I – average measurements, *ASME Transactions, Journal of Turbomachinery*, Vol. 118, pp. 562–569.

Hedman, A. (1994) Hydrodynamic torque converters in mechanical transmission systems: Methods and analysis, *ASME International Gas Turbine and Aeroengine Congress and Exposition, ASME Paper No.* 94-GT-285.

Marathe, B.V. and Lakshminarayana, B. (1995) Experimental investigation of steady and unsteady flow field downstream of an automotive torque converter turbine and stator, *International Journal of Rotating Machinery*, Vol. 2, pp. 67–84.

Marathe, B.V., Lakshminarayana, B. and Dong, Y. (1996) Experimental and numerical investigation of stator exit flow field of an automotive torque converter, *ASME Transactions, Journal of Turbomachinery*, Vol. 118, pp. 835–843.

Miner, S.M., Beaudoin, R.J. and Flack, R.D. (1989) Laser velocimetry measurements in a centrifugal flow pump, *ASME Transactions, Journal of Turbomachinery*, Vol. 111, pp. 205–212.

Schultz, H., Greim, R. and Volgmann, W. (1994) Calculation of three dimensional viscous flow in hydrodynamic torque converters, *ASME International Gas Turbine and Aeroengine Congress and Exposition, ASME Paper No.* 94-GT-208.

Stodola, A. (1945) *Steam and Gas Turbines*, Peter Smith Publisher, Gloucester, Mass.

Wiesner, F.J. (1967) A review of slip factors for centrifugal impellers, *ASME Transactions, Journal of Engineering for Power*, Vol. 89, pp. 558–572.

Watanabe, H., Kurahashi, T. and Kojima, M. (1997) Flow visualization and measurement of torque converter stator blades using a laser sheet lighting method and a laser velocimeter, *SAE Paper No.* 970680.

MANEY
publishing

The Institute of Materials, Minerals & Mining

ENERGY MATERIALS

NEW FOR 2006

Materials Science & Engineering for Energy Systems

Maney Publishing on behalf of the Institute of Materials, Minerals and Mining

Economic and environmental factors are creating ever greater pressures for the efficient generation, transmission and use of energy. Materials developments are crucial to progress in all these areas: to innovation in design; to extending lifetime and maintenance intervals; and to successful operation in more demanding environments. Drawing together the broad community with interests in these areas, *Energy Materials* addresses materials needs in future energy generation, transmission, utilisation, conservation and storage. The journal covers thermal generation and gas turbines; renewable power (wind, wave, tidal, hydro, solar and geothermal); fuel cells (low and high temperature); materials issues relevant to biomass and biotechnology; nuclear power generation (fission and fusion); hydrogen generation and storage in the context of the 'hydrogen economy'; and the transmission and storage of the energy produced.

As well as publishing high-quality peer-reviewed research, *Energy Materials* promotes discussion of issues common to all sectors, through commissioned reviews and commentaries. The journal includes coverage of energy economics and policy, and broader social issues, since the political and legislative context influence research and investment decisions.

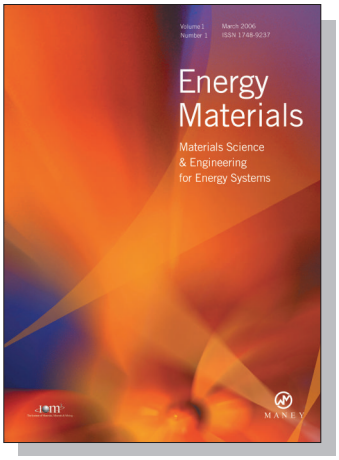

CALL FOR PAPERS

Contributions to the journal should be submitted online at **http://ema.edmgr.com**

To view the Notes for Contributors please visit: **www.maney.co.uk/journals/notes/ema**

Upon publication in 2006, this journal will be available via the Ingenta Connect journals service. To view free sample content online visit: **www.ingentaconnect.com/content/maney**

SUBSCRIPTION INFORMATION

Volume 1 (2006), 4 issues per year
Print ISSN: 1748-9237 Online ISSN: 1748-9245
Individual rate: £76.00/US$141.00
Institutional rate: £235.00/US$435.00
Online-only institutional rate: £199.00/US$367.00
For special IOM^3 member rates please email **subscriptions@maney.co.uk**

For further information please contact:
Maney Publishing UK
Tel: +44 (0)113 249 7481 Fax: +44 (0)113 248 6983 Email: subscriptions@maney.co.uk
or
Maney Publishing North America
Tel (toll free): 866 297 5154 Fax: 617 354 6875 Email: maney@maneyusa.com

For further information or to subscribe online please visit
www.maney.co.uk